



# New Synthetic Non-toxic Mono-azo Acid Dyes with Prominent Antibacterial Properties for Potential Application on Polyamide Fabrics

Muhammad Sohail Khan Rafiq<sup>1</sup> · Abdul Jabbar<sup>1,2</sup> · Saira Faisal<sup>3</sup> · Muhammad Salman<sup>1</sup>

Received: 2 November 2023 / Revised: 9 May 2024 / Accepted: 18 June 2024 / Published online: 11 July 2024  
© The Author(s), under exclusive licence to the Korean Fiber Society 2024

## Abstract

In pursuit of improving dyeability and incorporating antimicrobial attributes into polyamide fabric, a series of mono-azo acid dyes (SN1–SN5) were synthesized. Sulfathiazole was employed as an intermediate in the synthesis process of the dyestuff. The resultant dyes were characterized by employing various analytical techniques. The antimicrobial efficiency of these colorant was established through testing against *Aspergillus fumigatus*, *Staphylococcus aureus*, and *Escherichia coli*, displaying a spectrum of mild to strong antibacterial activity. Dye SN5 exhibited the highest potency, showing growth inhibition of 90% and 95% against both bacterial strains, respectively. Since the acid dyes are the prime contenders for utilization in food, pharmaceuticals, and cosmetics, an assessment was conducted on BJ Human Fibroblast Cells to evaluate any plausible adverse impacts. The results revealed that all the dyes exhibited no cytotoxicity. The dyeing properties of these colorants, including color representation, build-up, exhaustion, and fixation, were thoroughly examined following their application on the fabrics. The fastness properties were found to be considerably good to excellent. The influence of acidic and alkaline conditions on the absorption maxima was also explored. The dye SN3 showed a substantial bathochromic shift with increase in the solution's acidity in comparison to other dyes.

**Keywords** Mono-azo acid dyes · Sulfonamide dyes · Sulfathiazole · Antimicrobial activity · Cytotoxicity · pH sensitivity

## 1 Introduction

Azo dyes emerge as the largest category of synthetic dyes, dominating both in terms of quantity and commercial production. They are cost-effective to synthesize and exhibit excellent color strength [1]. Azo acid dyes are used to impart color to polyamide materials, such as nylon, natural protein fibers like wool, silk, acrylics, and fiber blends made from these fibers. These colorants function by forming electrostatic interactions with the positively charged ammonium groups in the fibers in acidic medium, providing reasonable colorfastness to light and laundry [2–4]. Their versatile applications extend beyond textiles as the vibrant colors

and excellent water solubility make these dyes suitable for application in cosmetics, leather, food, and pharmaceuticals. Moreover, they serve as integral components in advanced technologies, such as laser dyes, thermal transfer printing, fuel cells, and liquid crystal displays [5–9]. Contrary to these excellent and advantageous applications, azo acid dyes do have certain limitations. One notable constraint is their restricted applicability to materials beyond polyamides and protein fibers. Additionally, certain acid dyes may exhibit color fastness issues in specific conditions, such as exposure to light or harsh washing, resulting in gradual fading [5, 10]. It has been demonstrated that the incorporation of heterocyclic systems in the structure of azo dye can offer a larger spectrum of hues, improved color fastness, thermal stability, and tinctorial strength. These qualities can increase their affordability and sustainability [11–13]. It has also been found that some of the heterocyclic compounds are naturally bioactive. Hence, incorporating them in the azo dyes can produce colors with distinctive biological functionalities, such as antioxidant, antibacterial, antifungal, etc. These characteristics have made dyes with heterocyclic diazo components quite popular [13–17].

✉ Abdul Jabbar  
doctorjabbar@hotmail.com

<sup>1</sup> International Center for Chemical and Biological Sciences, H.E.J. Research Institute of Chemistry, University of Karachi, Karachi, Pakistan

<sup>2</sup> Textile Institute of Pakistan, Karachi, Pakistan

<sup>3</sup> NED University of Engineering and Technology, Karachi, Pakistan

The permeable nature of textile clothing facilitates the absorption of dirt, moisture, and food particles, thereby creating a favorable environment for the growth of microorganisms, which can lead to foul odor, brittleness of fabric, and potential infections in humans [18]. Several techniques have been developed to tackle these textile and health-related issues with the objective of endowing textiles with antimicrobial characteristics. These techniques include introduction of adsorbent substances into the fabric, applying active compounds as coatings, and fixing antimicrobial agents during the finishing stages [19]. These methods, however, are not well-suited for extended fabric use and are known for their elevated energy requirements, cost, and time-consuming nature. Hence, it is important to develop a strategy that enables the simultaneous operation of two energy-intensive processes; dyeing and antimicrobial finishing. In light of the market value of acid dyes and the available literature on the pharmacological properties of sulfathiazole, a set of mono-azo acid dyes (SN1–SN5) based on sulfathiazole have been synthesized (Scheme 1) [20–25]. The purpose of this study was to develop dyes with the dual capability of coloring polyamide textiles, including wool and nylon, while simultaneously exhibiting inherent antimicrobial properties and enhanced fastness. This approach not only addresses sustainability concerns but also offers clear advantages in terms of time and cost-effectiveness, making it a compelling strategy in textile manufacturing. The structures of all the synthesized colorants were validated via comprehensive spectroscopic analyses, while their cytotoxicity and antimicrobial efficacy were evaluated using the established methods. The color fastness attributes of the resultant acid dyes were carefully assessed according to ISO standards. The results indicated the performance levels ranging from good to excellent. An investigation into the thermal stability of these dyes was also conducted, exhibiting satisfactory results.

## 2 Experimental section

### 2.1 Materials and Instrumentation

Knitted wool cloth was procured from Askari Woolen Mills (Lahore) and had a GSM of 350 g/m<sup>2</sup>. From the local market, nylon-6 fabric with a GSM of 294.26 g/m<sup>2</sup> was purchased, and its purity was confirmed. Both the fabrics were solomatically bleached before use, ensuring they were clean and ready for dyeing with the synthesized dyes. Sulfathiazole sodium salt (**1**) was procured from Sigma Aldrich (USA). The coupling components (**2–6**) were acquired from Tokyo Chemical Industry (TCI) Japan. The chemicals mentioned in Fig. 1 were of lab grade and there was no need of any further purification step.

A Cecil 7400 UV–Visible spectrophotometer with a path length of 1 cm and dye concentrations ranging from

10<sup>−4</sup> M to 10<sup>−5</sup> M was used to measure the UV–Visible absorption spectra of all the synthetic dyes (SN1–SN5). With DMSO-*d*<sub>6</sub> and MeOH-*d*<sub>4</sub> as the solvents, the <sup>1</sup>H NMR spectra were recorded using Bruker Avance AV-400, 500 and 800 NMR spectrophotometers. In order to record the infrared (IR) spectra of the samples, the Shimadzu 8900 spectrophotometer was used. Prior to recording the spectra, the samples were mixed with powdered KBr, and the resultant blend was compacted to create consistent thin disks. A Bruker Amazon Speed mass spectrometer was used for the mass analysis, which made it possible to determine the mass-to-charge ratios of the synthesized dyes with accuracy and high precision. The wash fastness of the dyed textiles was evaluated using the Roaches Washtec-PA2, which provided insightful data on the color retention and resistance to fading after multiple washing cycles. The Crockmeter of SDL ATLAS CM-5 was used to measure the rubbing fastness of the dyed textiles, providing a precise and consistent evaluation of the fabric's resistance to color transfer or rubbing during normal use or handling. Use of the infra-red dyeing machine (IR Pyrotec MB) from Roaches, which offered effective and regulated dye penetration through the use of infrared radiation, was made to apply dyes to the fabric. The color strength (K/S) of the dyed samples was assessed using the Datacolor SF 650 spectrophotometer. An Advance Dyeing Solution Perspirometer, which enables controlled and standardized testing under circumstances simulating exposure to water and perspiration, was used to evaluate the water and perspiration fastness of the colored samples. The Air-Cooled Q-Sun Light Fastness Tester was used to test the light fastness of the colored textiles. A D180-P CO<sub>2</sub> incubator was used for BJ cell culture development, which enabled the growth and survival of the cells by providing a steady and regulated atmosphere of carbon dioxide (CO<sub>2</sub>), temperature, and humidity. The absorbance of the samples in a 96-well microplate was measured using a microplate reader, allowing for high-throughput analysis of multiple samples at once.

### 2.2 Synthesis of Acid Dyes (SN1–SN5)

#### 2.2.1 Diazotization Reaction

10 ml of HCl (20%) was used to dissolve sulfathiazole sodium salt (**1**) (2.0 mmol) during the synthesis procedure, and the reaction temperature was gradually lowered to 0–5 °C. Subsequently, a cold solution (10 ml) of sodium nitrite (2.2 mmol) was added dropwise to the reaction mixture over a period of 15 min with constant stirring. The start of the diazotization process was signaled by a change in the hue of the reaction mixture. The reaction mixture was continuously

stirred for approximately an hour, giving the diazotization reaction enough time to complete. The reaction was monitored by TLC using a dichloromethane:methanol solvent system in a 3:2 (v/v) ratio on aluminum oxide [18].

### 2.2.2 Coupling Reaction

The coupling component (2.0 mmol), dissolved in a 10 ml mildly basic solution (pH=7.5–8.5) of  $\text{Na}_2\text{CO}_3$ , was cooled to 0–5 °C. The cold coupling component solution was added dropwise to the previously synthesized diazonium salt solution with continuous stirring. After adjusting the pH to a range of 3–4, using a 2 M solution of  $\text{Na}_2\text{CO}_3$ , the reaction mixture was stirred for a duration of 2–3 h at a temperature of 0–5 °C. The progress of the reaction was supervised by TLC analysis with DCM: MeOH (6:4 v/v) as a solvent system. After completion of the reaction, HCl was added dropwise to salt out the synthetic colorants. The precipitated dye was removed using a filter paper, rinsed with 10% NaCl solution, and then dried in air [19].

### 2.2.3 Purification

The resulting crude dye was first subjected to a two-step washing procedure to remove both polar and non-polar impurities. The dye was initially rinsed with a 10% cold NaCl solution to get rid of any polar impurities, and then it was washed with dichloromethane (DCM) to get rid of any non-polar impurities. A saturated solution of the resultant dyes in methanol was prepared in order to further purify them. Ethyl acetate was then progressively added to the solution drop by drop. Following this cautious addition, the pure dye components began to precipitate from the solution. When the precipitation was finished,

the precipitated dyes were filtered from the remaining solution with a filter paper [26].

## 2.3 Characterization of the Synthesized Dyes (SN1–SN5)

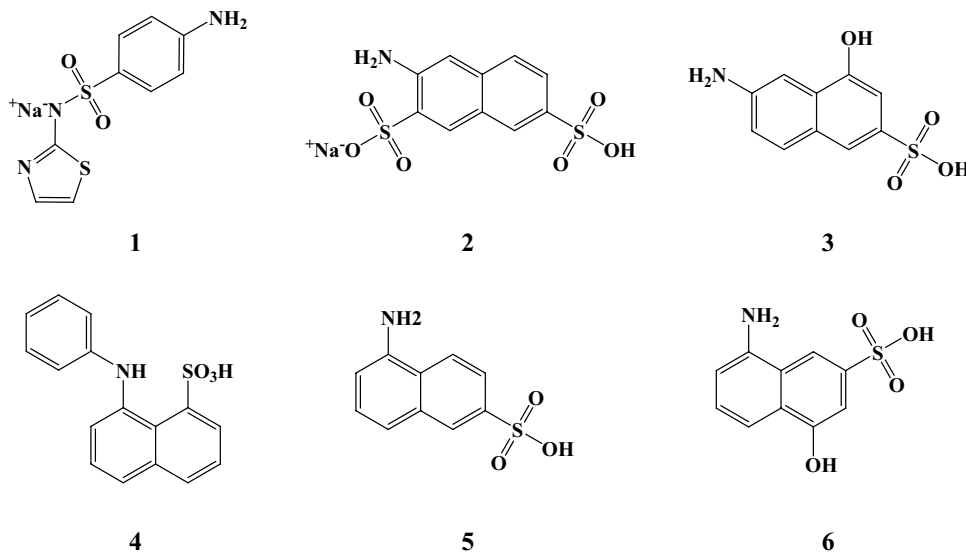
### 2.3.1 SN1: (E)-3-Amino-4-((4-(N-(Thiazol-2-yl)Sulfamoyl)Phenyl)Diazenyl)Naphthalene-2,7-Disulfonic Acid

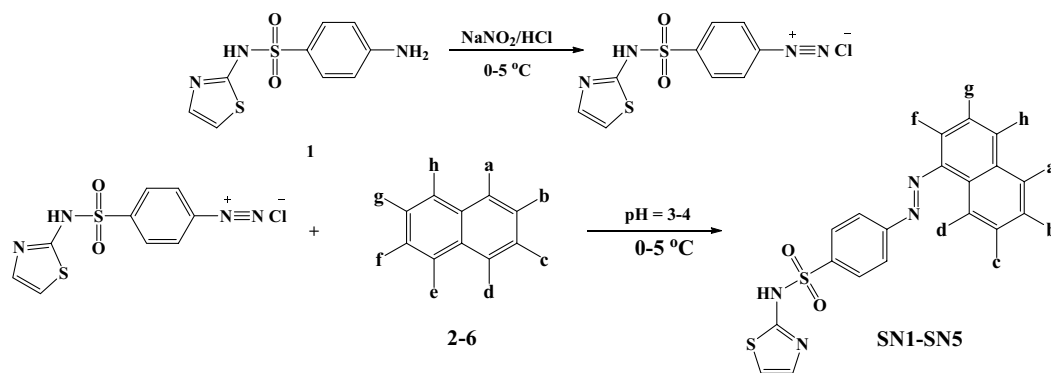
Orange solid; Yield: 89%; FT-IR (KBr,  $\text{cm}^{-1}$ ): 3424.09 ( $\text{NH}_2$ ), 1589.0 ( $\text{C}=\text{N}$ ), 1541.0 ( $\text{C}=\text{C}$ ), 1412.23 ( $\text{N}=\text{N}$ ), 1341.0 and 1150.0 ( $\text{S}=\text{O}$ ), 1342.02 ( $=\text{C}-\text{N}$ ).  $^1\text{H}$  NMR (DMSO- $d_6$ , 800 MHz,  $\delta$ ): 12.8 (1H, s, -NH-), 10.8 (1H, s, -NH-), 8.63 (1H, d,  $J=8.0$  Hz, H-5), 8.22 (1H, s, H-1), 8.04 (2H, d,  $J=8.8$  Hz, H-3', 5'), 7.97 (1H, br. s, H-8), 7.94 (2H, d,  $J=8.8$  Hz, H-2', 6'), 7.76 (1H, dd,  $J_{1,2}=1.0$  Hz,  $J_{1,3}=8.0$  Hz, H-6), 7.26 (1H, d,  $J=4.0$  Hz, H-4''), 6.85 (1H, d,  $J=4.0$  Hz, H-5'').  $^{13}\text{C}$ -NMR (800 MHz, DMSO- $d_6$   $\delta$ ): 108.38 (1C, C-5''), 120.57 (1C, C-5), 121.74 (2C, C-2', 6'), 123.69 (1C, C-9), 124.54 (1C, C-4''), 125.51 (1C, C-8), 126.10 (1C, C-6), 126.47 (1C, C-10), 127.17 (2C, C-3', 5'), 132.83 (1C, C-1), 134.47 (1C, C-7), 135.44 (1C, C-2), 138.25 (1C, C-3), 141.48 (1C, C-4'), 143.35 (1C, C-4), 155.0 (1C, C-1'), 168.93 (1C, C-2'). ESI-MS:  $[\text{M}+\text{H}]^+ = m/z$  570.1. UV-Visible ( $\text{H}_2\text{O}$ ):  $\lambda_{\text{max}}=465.0$  nm,  $\epsilon_{\text{max}}=15,495.0$  L.  $\text{mol}^{-1}\cdot\text{cm}^{-1}$ .

### 2.3.2 SN2: (E)-6-Amino-4-Hydroxy-5-((4-(N-(Thiazol-2-yl)Sulfamoyl)Phenyl)Diazenyl)Naphthalene-2-Sulfonic Acid

Red solid; Yield = 90%; FT-IR (KBr,  $\text{cm}^{-1}$ ): 3421.87 ( $\text{NH}_2$  /OH), 1594.43 ( $\text{C}=\text{N}$ ), 1518.59 ( $\text{C}=\text{C}$ ), 1421.17 ( $\text{N}=\text{N}$ ) 1272.41 and 1186.90 ( $\text{S}=\text{O}$ ), 1232 ( $=\text{C}-\text{N}$ ).  $^1\text{H}$  NMR (DMSO- $d_6$ , 400 MHz,  $\delta$ ): 12.4 (1H, s, -NH-), 10.6

**Fig. 1** Structures of chemicals employed in the synthesis of acid dyes





Where;

**SN1:** a = c = d = h = **H**, b = **SO<sub>3</sub>H**, f = **NH<sub>2</sub>**, g = **SO<sub>3</sub>Na**

**SN2:** a = **OH**, b = d = g = h = **H**, c = **SO<sub>3</sub>H**, f = **NH<sub>2</sub>**

**SN3:** a = **SO<sub>3</sub>H**, b = c = d = f = g = **H**, h = **NHPh**

**SN4:** a = b = d = f = g = **H**, c = **SO<sub>3</sub>H**, h = **NH<sub>2</sub>**

**SN5:** a = c = f = g = **H**, b = **SO<sub>3</sub>H**, d = **OH**, h = **NH<sub>2</sub>**

**Scheme 1** Synthetic pathway of the target acid dyes (SN1–SN5)

(1H, s, -NH-), 10.4 (1H, s, -OH), 7.97 (2H, d,  $J = 8.4$  Hz, H-3', 5'), 7.89 (1H, d,  $J = 9.2$  Hz, H-8), 7.81 (2H, d,  $J = 8.4$  Hz, H-2', 6'), 7.53 (1H, d,  $J = 1.6$  Hz, H-1), 7.27 (1H, d,  $J = 4.4$  Hz, H-4''), 7.20 (1H, d,  $J = 1.6$  Hz, H-3), 7.17 (1H, d,  $J = 9.2$  Hz, H-7), 6.86 (1H, d,  $J = 4.4$  Hz, H-5''). ESI-MS:  $[M + H]^+ = m/z$  506.1. UV-Visible (H<sub>2</sub>O):  $\lambda_{\max} = 510.0$  nm,  $\epsilon_{\max} = 16,980.0$  L. mol<sup>-1</sup>.cm<sup>-1</sup>.

### 2.3.3 SN3: (E)-8-(Phenylamino)-5-((4-(N-(Thiazol-2-yl)Sulfamoyl)Phenyl)Diazenyl)Naphthalene-1-Sulfonic Acid

Red solid; Yield = 88%; FT-IR (KBr, cm<sup>-1</sup>): 3449.63 (NH<sub>2</sub>), 1597.46 (C=N), 1531.12 (C=C), 1424.89 (N=N), 1265.12 and 1173.89 (S=O), 1146.25 (=C-N). <sup>1</sup>H-NMR (DMSO-*d*<sub>6</sub>, 500 MHz,  $\delta$ ): 12.2 (1H, s, -NH-), 9.09 (1H, dd,  $J_{1,2} = 1.5$ ,  $J_{1,3} = 8.0$  Hz, H-4), 8.32 (1H, dd,  $J_{1,2} = 1.5$  Hz,  $J_{1,3} = 8.0$  Hz, H-2), 7.97–8.00 (3H, m, H-6, 3'', 5''), 7.94 (2H, d,  $J = 8.5$  Hz, H-2'', 6''), 7.65 (1H, t,  $J = 7.5$  Hz, H-3), 7.40–7.43 (3H, m, H-7, 3', 5'), 7.31 (2H, d,  $J = 7.5$  Hz, H-2', 6'), 7.27 (1H, d,  $J = 5.0$  Hz, H-4'''), 7.13 (1H, t,  $J = 7.5$  Hz, H-4'), 6.85 (1H, d,  $J = 5.0$  Hz, H-5'''). ESI-MS:  $[M + H]^+ = m/z$  566.2. UV-Visible (H<sub>2</sub>O):  $\lambda_{\max} = 517.0$  nm,  $\epsilon_{\max} = 17,280.0$  L. mol<sup>-1</sup>.cm<sup>-1</sup>.

### 2.3.4 SN4: (E)-5-Amino-8-((4-(N-(Thiazol-2-yl)Sulfamoyl)Phenyl)Diazenyl)Naphthalene-2-Sulfonic Acid

Red solid; Yield = 91%; FT-IR (KBr, cm<sup>-1</sup>): 3449.45 (NH<sub>2</sub>), 1595.17 (C=N), 1554.23 (C=C), 1426.86 (N=N), 1269.76 and 1169.19 (S=O), 1294.25 (=C-N). <sup>1</sup>H-NMR (500 MHz, DMSO-*d*<sub>6</sub>,  $\delta$ /ppm): 12.8 (1H, s, -NH-), 8.95 (1H, s, H-1), 8.28 (1H, d,  $J = 8.5$  Hz, H-4), 8.23 (1H, br. s, H-7), 7.96 (2H, d,  $J = 8.5$  Hz, H-3', 5'), 7.84 (2H, d,  $J = 8.5$  Hz, H-2', 6'), 7.78 (1H, d,  $J = 8.5$  Hz, H-3), 7.26 (1H, d,  $J = 4.5$  Hz, H-4''), 6.98 (1H, d,  $J = 7.5$  Hz, H-6), 6.84 (1H, d,  $J = 4.5$  Hz, H-5''). ESI-MS:  $[M + H]^+ = m/z$  490.2. UV-Visible (H<sub>2</sub>O):  $\lambda_{\max} = 497.5$  nm,  $\epsilon_{\max} = 12,750.0$  L. mol<sup>-1</sup>.cm<sup>-1</sup>.

### 2.3.5 SN5: (E)-8-Amino-4-Hydroxy-5-((4-(N-(Thiazol-2-yl)Sulfamoyl)Phenyl)Diazenyl)Naphthalene-2-Sulfonic Acid

Dark magenta solid; Yield = 90%; FT-IR (KBr, cm<sup>-1</sup>): 3449.10 (NH<sub>2</sub>/OH), 1593.52 (C=N), 1544.75 (C=C), 1451.83 (N=N), 1261.50 and 1135.40 (S=O), 1299.11 (=C-N). <sup>1</sup>H-NMR (500 MHz, MeOH-*d*<sub>4</sub>,  $\delta$ /ppm): 8.26 (1H, d,  $J = 8.5$  Hz, H-6), 8.06 (1H, d,  $J = 2.0$  Hz, H-1), 8.05 (2H, d,  $J = 8.5$  Hz, H-3', 5'), 7.69 (2H, d,  $J = 8.5$  Hz, H-2', 6'), 7.46 (1H, d,  $J = 2.0$  Hz, H-3), 7.04 (1H, d,  $J = 4.0$  Hz, H-4''), 6.84 (1H, d,  $J = 8.5$  Hz, H-7), 6.58 (1H, d,  $J = 4.0$  Hz, H-5''). ESI-MS:  $[M + H]^+ = m/z$  506.2. UV-Visible (H<sub>2</sub>O):  $\lambda_{\max} = 519.0$  nm,  $\epsilon_{\max} = 10,470.0$  L. mol<sup>-1</sup>.cm<sup>-1</sup>.

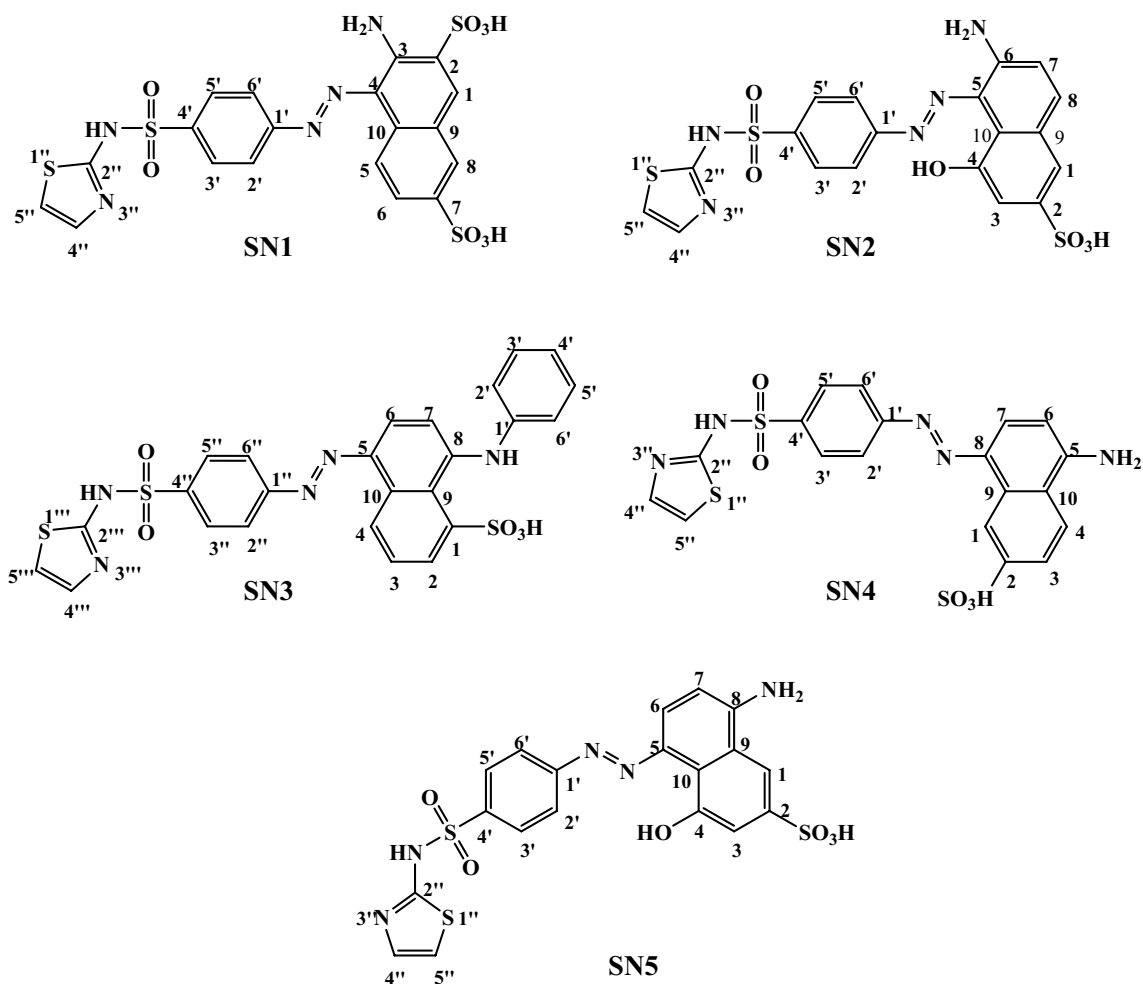


Fig. 2 Structures of the resultant acid dyes (SN1–SN5)

## 2.4 Biological Studies

### 2.4.1 Cytotoxicity Screening of the Synthesized Acid Dyes (SN1–SN5)

The standard 3-(4,5-dimethylthiazol-2-yl)-2,5-diphenyltetrazolium bromide (MTT assay) was used to assess the cytotoxic activity of the dyes in a flat-bottomed 96-well plate. In order to do this, BJ *Human Fibroblast Cells* were grown in the culture medium which comprised of 10% fetal bovine serum (FBS), 100 g/ml of streptomycin, and 100 IU/ml of penicillin in addition to Dulbecco's Modified Eagle media, and 2 mM glutamine in 75 cm<sup>2</sup> flasks, and maintained in a 5% CO<sub>2</sub> incubator at 37 °C. Cells that were exponentially proliferating were collected, counted using a hemocytometer,

and diluted with a specific medium. 100 µl/well of the prepared cell culture containing 6 × 10<sup>4</sup> cells/ml was added to 96-well plates. After allowing for an overnight incubation, the preceding medium was eliminated, and 200 µl of new media containing varying concentrations of the compounds (ranging from 1 to 30 µM) was introduced. After 48 h, each well was treated with 200 µl of MTT solution (0.5 mg/ml) and incubated for an additional 3 h. Subsequently, 100 µl of DMSO was introduced into each well, and the microplate reader was employed to quantify the reduction of MTT to formazan within the cells by measuring the absorbance at 550 nm. For BJ cells, the cytotoxicity was assessed based on the concentration that induced a 50% growth inhibition. (IC<sub>50</sub>). Using the formula given in Eq. 1, the percent inhibition was determined [27–29].

$$\%Inhibition = 100 - \left( \frac{\text{Mean of O.D of test compound} - \text{mean of O.D of negative control}}{\text{Mean of O.D of positive control} - \text{mean of O.D of negative control}} \times 100 \right) \quad (1)$$

The data (% inhibition) were processed using Soft-Max Pro software (Molecular Device, USA).

#### 2.4.2 Determination of Antimicrobial Activity of the Dyes

Antifungal activity was assessed using the agar tube dilution method. Sabouraud dextrose agar (10ml) was poured into tubes with screw caps and autoclaved for 21 min at 121 °C. After allowing the tubes to cool at 50 °C, the agar was loaded with 3mg/ml of sample solutions. After that, at room temperature, the tubes containing the media were positioned in a slanting manner to allow solidification. Fully grown culture of *Aspergillus fumigatus* was used to inoculate the tubes containing solidified media and the test samples, using a fungal inoculum measuring 4 mm in diameter. As a positive control, one tube of the standard medication Amphotericin B was prepared, while slants containing solely DMSO were utilized as a negative control. The test tubes were subjected to an incubation period of three days at a temperature of 28 °C. After the incubation period, the fungal linear length (measured in millimeters) was assessed, and the degree of growth inhibition was determined by comparing it to the control samples. Using the formula in Eq. 2, the percent growth inhibition (% GI) was computed [30, 31].

$$\%GI = 100 - \left( \frac{\text{Linear growth in test (mm)}}{\text{Linear growth in control (mm)}} \times 100 \right) \quad (2)$$

The disk diffusion method was used for the assessment of antibacterial activity of the synthesized dyes. Using a sterile swab, bacterial cultures of *Escherichia coli* and *Staphylococcus aureus* were evenly inoculated onto separate plates containing Mueller–Hinton agar. The disks were laid out on the agar surface after being impregnated with dye samples. A standard commercial antibiotic (Ofloxacin) disk served as the positive control and a disk soaked with DMSO only served as a negative control. Depending on the type of bacteria employed in the test, the plates were incubated at 37°C for a specific period. After the incubation period, the formula given in Eq. 3 was used to calculate the percent growth inhibition (%GI) of the dyes against each bacterium [23].

$$\%GI = \frac{C - T}{C} \times 100 \quad (3)$$

where T = microbial growth in treated plates (mm) and C = microbial growth in control plates (mm).

#### 2.4.3 Build-up Study of the Synthesized Dyes (SN1–SN5)

The fabrics (wool and nylon-6) were treated with the synthesized dyes at various concentrations, ranging from 1 to 5% *owf* (On Weight of Fabric), and the pH was maintained within the range of 3–5. The applied concentrations of these synthesized dyes were graphed against the maximum color strength values (K/S) to establish build-up profile of the dyes. Color strength levels (K/S) were calculated using the Kubelka–Munk equation (Eq. 4). The build-up profile technique optimizes the dyeing process for achieving precise, consistent, and appealing color results.

$$\frac{K}{S} = \frac{(1 - R)^2}{2R} \quad (4)$$

where K = absorbance coefficient. S = scattering coefficient. R = reflectance ratio.

#### 2.5 Exhaust Dyeing of Wool and Nylon-6 with the Dyes (SN1–SN5)

The synthetic acid dyes (SN1–SN5) were used to dye wool and nylon-6 textiles at 4% *owf* (On Weight of Fabric) shade depth. In the exhaust dyeing process, a liquor ratio of 1:10 was employed, while the pH was kept within the range of 3–5. To make the fiber dyeable with anionic acid dyes, dilute acetic acid was used to protonate the fiber. The fabric was submerged in the dye solution present in the dyeing container, which was then placed in the dyeing machine at a temperature of 35 °C. The temperature was gradually increased to 80 °C and kept there for one hour. The temperature was dropped to 35 °C when the dwell period was over. From the containers, the colored specimens were retrieved, rinsed with cold and hot water, and then dried in air [32]. Figure 3 shows the dyed fabric samples and solutions of the synthesized acid dyes.

Using the formula in Eq. 5, the fixation of the dyes on the fabric was assessed from the K/S values before [(K/S)<sub>1</sub>] and after [(K/S)<sub>2</sub>] washing with hot water.

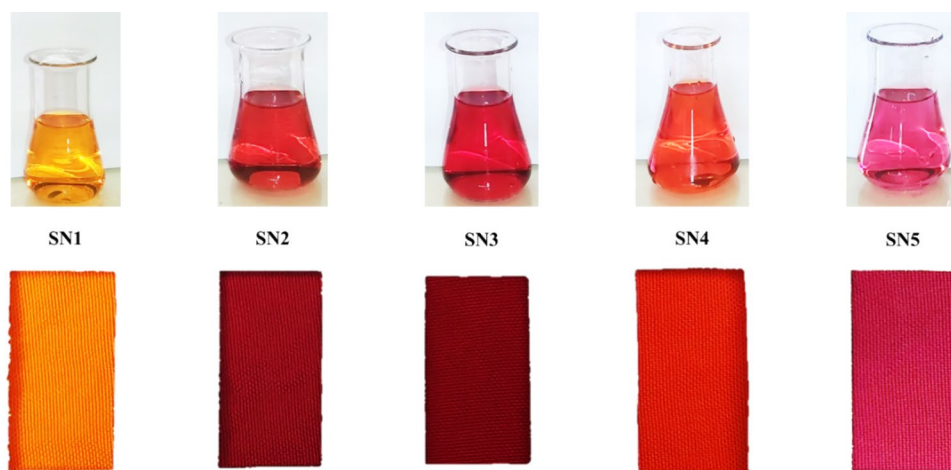
$$\%F = [(K/S)_2 / (K/S)_1] \times 100 \quad (5)$$

Equation 6 was employed to determine the % exhaustion after measuring the dye solution's absorbance both before and after dyeing.

$$\%E = [1 - (A_2/A_1)] \times 100 \quad (6)$$

Using the formula mentioned in Eq. 7, the dyes' total fixing percentage was also determined.

**Fig. 3** Dyed fabric samples and solutions of the synthesized acid dyes (SN1–SN5)



$$\%T = \frac{\%E \times \%F}{100} \quad (7)$$

## 2.6 Fastness Evaluation

Several fastness tests of the dyed fabric were conducted using ISO standard procedures which specifies methods used to assess the effect on the color of textiles upon exposure to different environmental factors. According to ISO 105-B02:2014, the fastness to light was assessed. The ISO 105-X12: 2010 technique was used to evaluate rubbing fastness. To determine wash fastness, a standard test procedure according to ISO 105-C06: 1994-A1S was used. The fastness to perspiration and the fastness to water were assessed employing ISO 105-E04: 1996 and ISO 105-E01: 1996, methods respectively. The ISO gray scale grading was used to rate the fastness outcomes.

## 2.7 Thermal Stability of the Dyes

In the TGA experiment, the sample was placed in a crucible and positioned inside a specialized apparatus called a thermogravimetric analyzer. The temperature of the sample was then changed in accordance with a predetermined temperature program. The program involved a gradual increase in the temperature from 50 °C to 950 °C at a rate of 15 °C/min. The weight change was tracked throughout the program [20].

# 3 Results and Discussion

## 3.1 Synthesis and Spectral Interpretations

By following the methodology detailed in Sect. 2.2, a series of mono-azo acid dyes were synthesized. The initial step involved a reaction carried out at low temperature (0–5 °C),

resulting in the formation of a diazonium salt from sulfathiazole. In the subsequent coupling step, the diazonium salt was reacted with naphthalene derivatives at a pH range of 3–4 and temperature of 0–5 °C. Through the use of various spectroscopic methods, the structures of the resultant colorants (SN1–SN5) were confirmed. These techniques include FT-IR, ESI-MS, NMR, and electronic absorption spectroscopy. The IR spectra of all the dyes had distinctive broad bands in the region of 3440  $\text{cm}^{-1}$ , which correspond to the stretching vibrations of amino and hydroxyl groups that are hydrogen bonded. The distinctive azo ( $-\text{N}=\text{N}-$ ) functional group peaks were found in the region of 1420  $\text{cm}^{-1}$ , which validate the synthesis of the desired compounds. The spectral bands within the range of 1550–1600  $\text{cm}^{-1}$  were assigned to the stretching vibrations associated with the  $\text{C}=\text{N}$  bonds, while the peak for aromatic  $\text{C}=\text{C}$  stretching vibrations was observed at around 1550  $\text{cm}^{-1}$  region. Peaks corresponding to the symmetric and asymmetric stretching vibrations of  $\text{S}=\text{O}$  were identified within the spectral range of 1100.0 and 1300.0  $\text{cm}^{-1}$ , respectively. The expected molecular masses of all the dyes were confirmed through electrospray ionization mass spectrometry. The  $^1\text{H}$  NMR spectra were also in good association with the predicted structures cited in Fig. 2. All the aromatic protons were recorded in the range of 6.5–9.1 ppm with respective multiplicities. The origin of the downfield resonance within the 9.0 to 13.0 ppm range was attributed to the H-bonded protons of the amine or hydroxyl group. According to the literature, the usual (non-H-bonded)  $\text{NH}_2$  and OH protons appear before the aromatic region but H-bonding alter the electron density distributions within the molecules, which can have a variety of implications on molecular characteristics like bond lengths and NMR signals [33, 34]. Analysis of the  $^1\text{H}$  NMR spectra of the dyes SN1 and SN2 revealed the presence of two separate singlet signals in the range of 10–13 ppm. These signals were due to the imine and azonium protons respectively, affirming the prevalence of

hydrazo (azonium) tautomeric form of these dyes. This conclusion gained additional support from the results of the electronic absorption study. The  $^{13}\text{C}$ -NMR (broadband) spectrum of **SN1** dye displayed signals corresponding to all 19 carbon atoms at their specific positions. The carbon 2'' attached to three heteroatoms was observed at 168.9 ppm. The assigned values were confirmed through the 2D-COSY, TOCSY, HSQC, and HMBC correlations. The COSY spectrum showed correlations of H-5 ( $\delta$  8.63) with H-6 ( $\delta$  7.76), H-3', 5' ( $\delta$  8.04) with H-2', 6' ( $\delta$  7.94), H-8 ( $\delta$  7.97) with H-6 ( $\delta$  7.76), and H-4'' ( $\delta$  7.26) with H-5'' ( $\delta$  6.85). Through TOCSY spectrum, the correlation between H-5 ( $\delta$  8.63) and H-8 ( $\delta$  7.97) was confirmed. The HSQC spectrum of **SN1** dye also revealed the heteronuclear  $^1\text{H}$ - $^{13}\text{C}$  interactions for all the protons that are directly bonded to the carbon atoms, while quaternary carbon's chemical shift values were confirmed through HMBC spectrum. In the HMBC spectrum, both H-4'' ( $\delta$  7.26) and H-5'' ( $\delta$  6.85) protons showed interaction with C-2'' ( $\delta$  168.9) carbon. The H-6 ( $\delta$  7.76) proton showed interaction with C-5 ( $\delta$  120.57), C-7 ( $\delta$  134.47), and C-8 ( $\delta$  125.51). H-1 ( $\delta$  8.22) experienced interaction with C-9 ( $\delta$  123.69), C-2 ( $\delta$  135.44), and C-3 (138.25). Similarly, the H-5 proton showed three bonds correlation with C-9 ( $\delta$  123.69), two bond with C-10 ( $\delta$  126.47), and a three bonds correlation with C-4 ( $\delta$  143.35). The H-2', 6' ( $\delta$  7.94) protons experienced a two bonds interaction with C-1' ( $\delta$  155.0), while the H-3', 5' ( $\delta$  8.04) protons interacted with C-4' ( $\delta$  141.48) carbon as shown in Fig. 4.

## 3.2 Electronic Absorption Study

### 3.2.1 Substituent Effect

The absorption spectra of the dyes **SN1** to **SN5** were recorded in distilled water, and the results are shown in Fig. 5. It was found that these dyes show absorbance in 465.0 to 520.0 nm range, resulting from the electronic transition of the azo group. The electron-donating groups in a molecule cause a bathochromic shift, as was previously recognized [35]. In comparison to **SN2** dye, which has one sulfonate group at carbon 2 and electron-donating hydroxyl and amino groups at carbons 4 and 6 respectively, **SN1** dye has two electron withdrawing sulfonate groups at carbons 2 and 7 and one electron-donating amino group at carbon 3. The presence of hydroxyl group and one sulfonate group less than that of **SN1** dye is responsible for the bathochromic shift in dye **SN2**. **SN1** dye absorbs at around 465.0 nm while **SN2** at 510.0 nm region. **SN3** dye has an extra phenyl ring attached to the nitrogen of amino group at carbon 8 and has a sulfonate group at carbon 1. The dye **SN2**, which has a hydroxyl group as an auxochrome that donates electrons, contrasts with dye **SN3**, which is devoid of this component. Nonetheless, because

the conjugation is extended by the presence of the phenyl ring, a bathochromic shift is still visible from the 510.0 nm region to the 517.0 nm region. Since dye **SN4** lacks the phenyl ring that **SN3** has, there is a hypsochromic shift from the region of 517.0 nm to 497.5 nm. Both **SN2** and **SN5** dyes have similar substituents, but the azo group in **SN2** is at ortho position to the amino group, whereas it is at para position in **SN5**, extending the conjugation between the auxochrome and chromophore. It explains why a bathochromic shift from the region of 510.0 to 519.0 nm was noticed upon comparison of the UV–Visible spectra of both these dyes.

### 3.2.2 pH Effect

It was observed that the position of absorption maxima of some of the synthesized dyes also depends on the pH of the medium as evident from the UV–Visible spectra of the dyes **SN3** and **SN5** shown in Figs. 6 and 7 respectively. Therefore, the electronic absorption spectra of all the synthesized dyes were studied in acidic, basic, and neutral media and the results are listed in Table 1. A key motif in the current discussion is the intramolecular hydrogen bond with changing structural and environmental elements (pH of the medium) during the tautomeric conversion process. It was observed that the structures of the dyes **SN1** and **SN2** allow the formation of intramolecular hydrogen bonding that favors the hydrazo (azonium) tautomer (**B**) more compared to the azo tautomer (**A**), that is why these dyes exist predominantly in hydrazo (azonium) form (**B**) irrespective of the pH of the medium. The tautomeric equilibrium depicted in the Fig. 8 is the main reason behind the absorption in the same region because all of the tautomers have identical  $\pi$ -bond order [36, 37] Fig. (9).

In case of dyes **SN3** and **SN4**, (Fig. 10) there is no intramolecular H-binding. Therefore, these dyes predominantly exist in the azo form (molecular form (**F**)) in neutral aqueous medium. In basic medium, the azo form (**F**) gets deprotonated resulting into an anionic form (**E**). Both of these azo (**F**) and anionic (**E**) forms absorb in almost similar region as shown in Fig. 6. In an aqueous acidic medium, a bathochromic shift was observed due to the hydrazo (azonium) form (**G**). The formation of a quinoid structure in the hydrazo (azonium) tautomer is responsible for the strong electronic delocalization. Among all the synthesized dyes, dye **SN3** showed significant bathochromic shift in acidic medium due to considerable increase in  $\pi$ -bond order compare to the other dyes. This is because **SN3** dye has an additional phenyl ring attached to the nitrogen of the amino group that can get involve in delocalization of electrons resulting into an extended conjugation [20, 21].

Dye **SN2** and dye **SN5** have similar structures, but the only difference is the position of (Fig. 11)  $\text{NH}_2$  group. In



**SN2**, the  $\text{NH}_2$  group is ortho to the azo group that facilitates the formation of intramolecular H-bonding with the  $\beta$ -nitrogen of the azo group while in **SN5**, it is para to the azo group, so the possibility of its involvement in intramolecular H-bonding with the  $\beta$ -nitrogen of the azo group is vanished. This is why its hydrazo (azonium) form (**J**) is only stable in acidic medium because the  $\beta$ -nitrogen of the azo group in acidic medium get protonated that pulls the electronic density resulting into the formation of hydrazo (azonium) tautomer. This is evident from the bathochromic shift observed when a few drops of concentrated HCl were added to its neutral solution. In neutral medium, the dye exists in its molecular form (**I**) while in basic medium, the anionic form (**H**) of the dye predominates. Both the molecular and anionic forms absorb in approximately same 515–519 nm region as evident from Fig. 7 [38–42].

### 3.3 Dyeing Performance of the Synthesized Dyes (SN1–SN5) on Wool and Nylon-6

In order to assess the build-up characteristics of the dyes, wool and nylon-6 fabrics were dyed at a number of percent shades (% *owf*) and their color strength values were recorded.

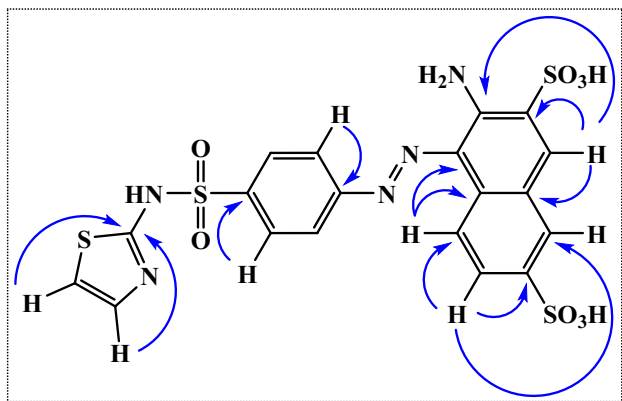
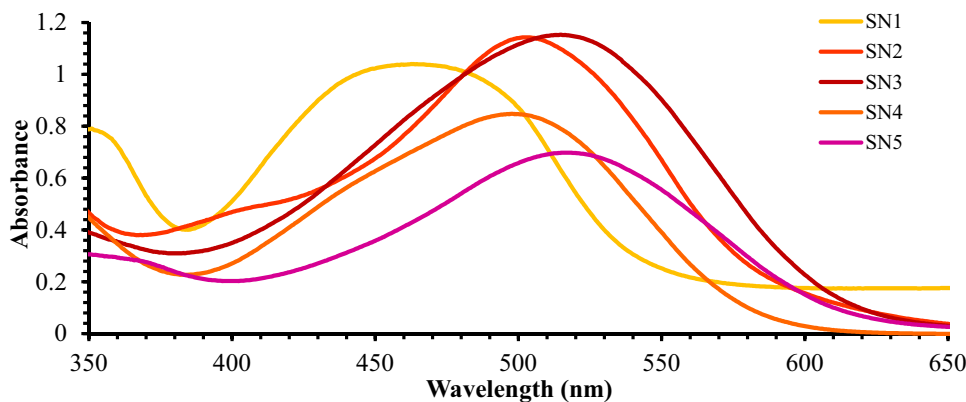


Fig. 4 HMBC correlations of the dye SN1

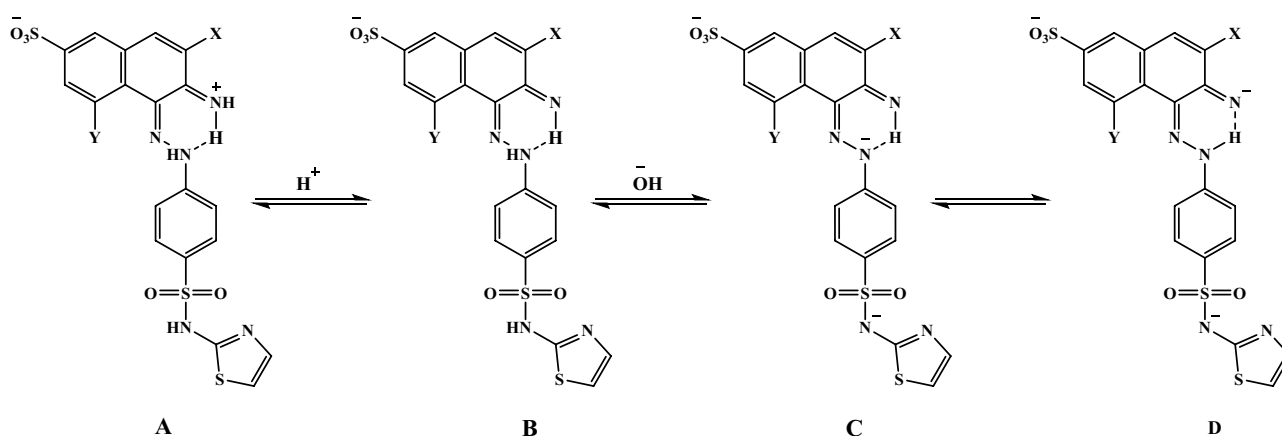
Fig. 5 UV–Visible spectra of the synthesized dyes



The results demonstrated a satisfactory build-up of all the colors on both materials. The K/S values grew linearly as the dye concentration increased from 1 to 4% *owf* concentration, as shown in Tables 2 and 3. When the dye was applied at a concentration of 4% of the fabric's weight (4% *owf*), which resulted in the fabric's color strength saturation, as there was no noticeable difference when the concentration was further raised from 4 to 5%. In other words, at this particular dye concentration, the fabric displayed the most intense and vivid color, signifying the maximum color strength saturation. It suggests that utilizing a higher concentration might produce dye aggregates on the fabric. Concentration of the dye lower than 4% *owf* will produce less intense colors with lower color strength. This information can help achieve the appropriate color intensity and optimization of the dyeing procedure.

Following a comprehensive build-up study, the exhaust dyeing procedure was used for the subsequent dyeing of wool and nylon-6 at a 4% *owf* shade depth using the synthetic dyes (SN1–SN5). Strong dye-fiber interactions are produced between the protonated polyamide fibers (wool and nylon-6) and the acid dye. In acidic medium, the acid dye's negatively charged sulfonate groups ( $-\text{SO}_3^-$ ) are drawn to and interact with the positively charged amine groups on the protonated polyamide fibers. These interactions aid in binding the dye molecules firmly to the fiber surface, making the dyeing process more durable and wash-resistant.

Depending on the presence of auxochrome and chromophore, all the dyes produced somewhat varying hues on the cloth (wool and nylon-6). Dye SN1 produced light orange, SN2 red, SN3 deep red, SN4 reddish orange, and SN5 magenta. The data in Tables 4 and 5 demonstrated that between wool and nylon-6 fabrics, these synthetic dyes showed a distinct difference in dye exhaustion, with wool performing relatively better. This finding can be explained by the fact that there are more dye binding sites ( $-\text{NH}_2$  groups) in wool than nylon-6. Since wool is a protein-based natural fiber, it has a more complex polymeric structure and



**SN1:** X = SO<sub>3</sub><sup>-</sup>, and Y = H

**SN2:** X = H, and Y = OH

**Fig. 6** Possible tautomeric structures of dyes **SN1** and **SN2**

**Fig. 7** UV-Visible absorption of the dye **SN1** in acidic, basic, and neutral media

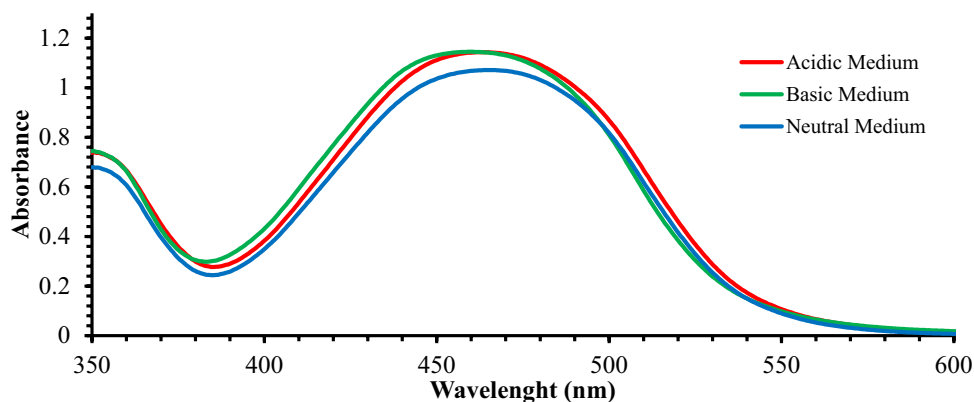


**Table 1**  $\lambda_{\max}$  of the synthesized dyes in acidic, basic, and neutral media

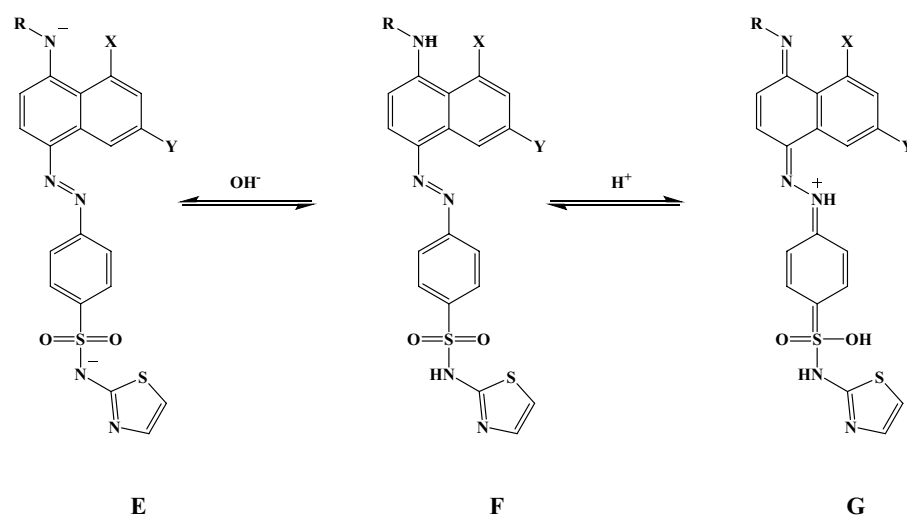
Dyes	$\lambda_{\max}$ (HCl + H <sub>2</sub> O) (nm)	$\lambda_{\max}$ (H <sub>2</sub> O) (nm)	$\lambda_{\max}$ (NaOH + H <sub>2</sub> O) (nm)
SN1	465.5	465.0	465.5
SN2	510.5	510.0	510.0
SN3	552.5	517.0	515.0
SN4	506.5	497.5	495.0
SN5	526.5	519.0	515.5

a lot of amino groups, which act as sites where dye molecules can chemically bind during dyeing [43].

### 3.3.1 Fastness Assessment Using ISO Standard Methods

All samples of the colored fabric were examined for color fastness using ISO standards. Gray scale ratings, which

range from 1 to 5 (where 5 is for excellent fastness) were used to evaluate the outcomes. In the case of nylon-6, the fabric's crystalline structure enables acid dyes to bind with the material effectively, making it hard for the dye molecules to escape the crystal lattice once they have been absorbed. Because of this, nylon-6 fabrics colored with these acid dyes exhibit better color fastness and maintained their color vibrancy even after several washings. However, despite the fact that wool is similarly receptive to acid dyes, but it does not offer the same level of color fastness as nylon-6. In comparison to nylon-6, wool fibers are more porous and had less crystallinity in its polymeric structure and can leak dye molecules over time as evident from the results [22, 43]. The color fastness results were also compared with the commercial acid dye (C.D) as shown in the Fig. 12. Dyes **SN1**, **SN3**, and **SN5** demonstrated fastness properties nearly identical to those of the commercial dye (C.D). Moreover, in specific aspects such as light fastness on wool fabric, dyes **SN1** and **SN3** surpassed the performance of the commercial



**SN3:** R = Ph, X = SO<sub>3</sub><sup>-</sup>, and Y = H

**SN4:** R = X = H, Y = SO<sub>3</sub><sup>-</sup>

**Fig. 8** Possible tautomeric structures of dyes SN3 and SN4

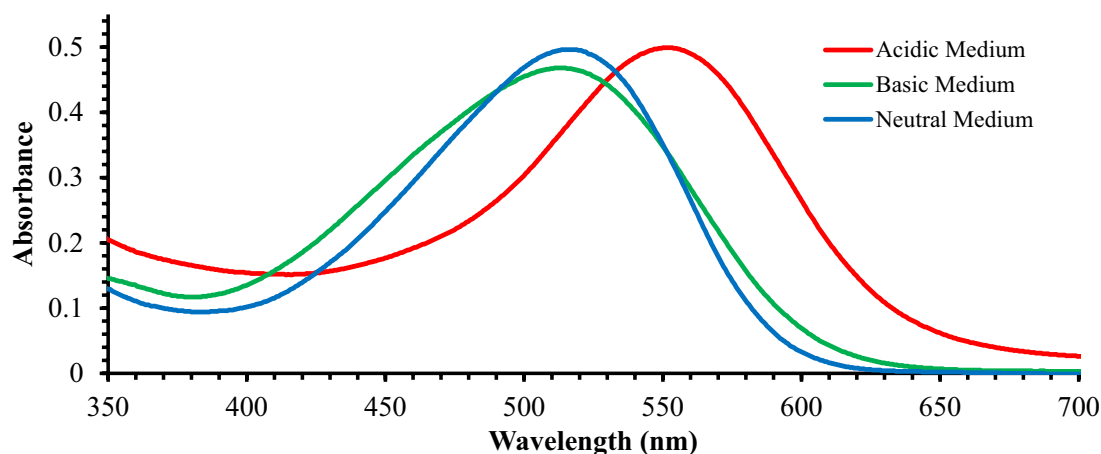


**Fig. 9** UV-Visible absorption of dye SN3 in acidic, basic, and neutral mediums

dye. These results underscore the potential of these synthetic dyes to either match or surpass the performance of commercially available dyes across various criteria, thereby indicating their suitability for industrial applications. Furthermore, it is noteworthy that the majority of the synthesized dyes (SN1–SN5) exhibit antimicrobial properties, a feature notably absent in most of the commercial dyes.

### 3.4 Biological Efficacy

#### 3.4.1 Cytotoxicity

The cytotoxicity of the synthesized dyes was determined using a known method discussed in Sect. 2.4. The concentration that causes a 50% reduction in cell growth was designated as the 50% inhibitory concentration (IC<sub>50</sub>) for a sample. The MTT colorimetric assay, relying on the metabolic activity of cells, involves the transformation of a yellow tetrazolium salt (MTT) into crystals of a purple formazan compound. In live cells, the NAD(P)H-dependent oxidoreductase enzymes facilitate the conversion of MTT

**Fig. 10** Possible tautomeric structures of dyes SN5

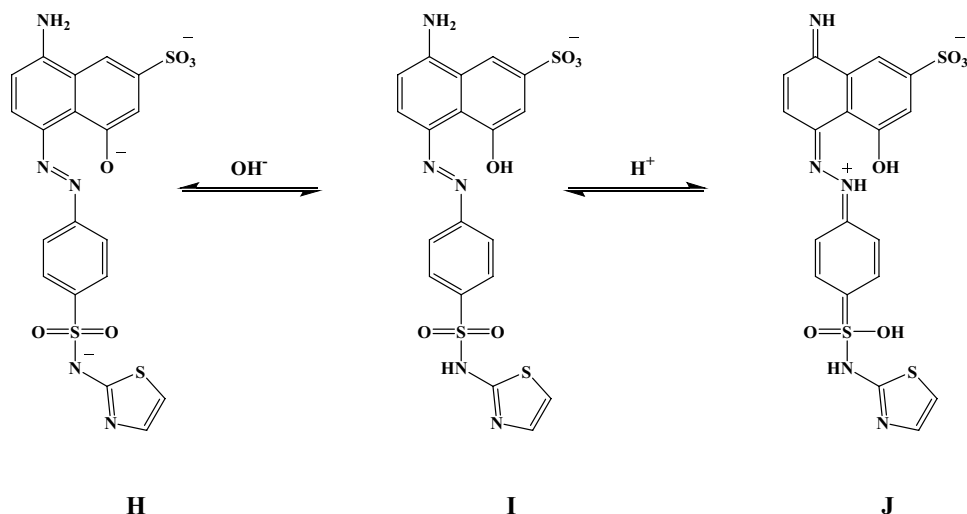


**Fig. 11** UV-Visible absorption of dye SN5 in acidic, basic and neutral mediums

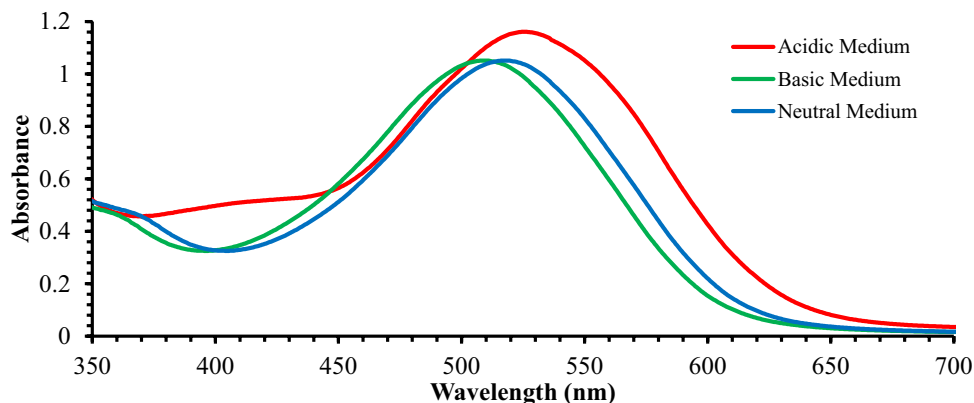


**Table 2** K/S values of the dyed wool fabric at different shade depth of the dye (*owf*)

% Shade	SN1	SN2	SN3	SN4	SN5
1	10.9	11.8	11.9	8.9	11.1
2	14.5	15.9	15.2	14.0	16.1
3	22.7	25.1	24.3	23.5	23.1
4	33.1	34.1	35.2	31.7	33.9
5	33.4	35.0	35.9	32.1	34.4

to formazan. To dissolve the insoluble formazan crystals, a solubilization medium like DMSO was employed, and the absorbance of the resulting colored solution was measured using a multi-well spectrophotometer. The solution's dark color signified the presence of large number of metabolically active and viable cells. This experiment was conducted to determine whether or not the fabric dyed with these dyes will impact the health of the end user. Additionally, the

**Table 3** K/S values of the dyed nylon-6 fabric at different shade depth of the dye (*owf*)

% Shade	SN1	SN2	SN3	SN4	SN5
1	8.9	9.8	11.7	9.1	11.9
2	12.6	15.1	16.8	11.3	14.1
3	21.9	23.8	24.4	20.1	23.1
4	31.2	33.9	34.1	29.1	33.2
5	32.1	34.2	34.6	29.9	33.7

potential application of these dyes in food, medicine, and cosmetics coloring was studied. The 50% inhibitory concentration ( $IC_{50}$ ) and the % inhibition/ stimulation (% I/S) values were determined and are listed in Table 6. All the dyes were found non-cytotoxic. The dye SN4 displayed the highest % I/S value, whereas dye SN5 exhibited the lowest value [28, 29].

**Table 4** Dyeing characteristics of the synthetic colorants (SN1–SN5) dyes on wool

Dye	%F	(K/S) <sub>1</sub>	(K/S) <sub>2</sub>	%E	%T
SN1	92.7	35.7	33.1	91.30	84.6
SN2	92.4	36.9	34.1	89.15	82.4
SN3	91.2	38.6	35.2	89.90	81.9
SN4	92.7	34.2	31.7	90.67	84.0
SN5	92.1	36.8	33.9	91.56	84.3

**Table 5** Dyeing characteristics of the synthetic colorants on nylon-6

Dye	%F	(K/S) <sub>1</sub>	(K/S) <sub>2</sub>	%E	%T
SN1	93.7	33.3	31.2	85.42	80.0
SN2	95.5	35.5	33.9	84.23	82.3
SN3	95.2	35.8	34.1	85.70	81.6
SN4	94.1	30.9	29.1	83.50	82.3
SN5	92.6	35.5	33.2	84.92	81.4

**3.4.2 Antimicrobial Efficacy of the Dyes (SN1–SN5)**

Antimicrobial efficacy (in vitro) of the dyes (SN1–SN5) was determined against *Aspergillus fumigatus*, *Escherichia coli*, and *Staphylococcus aureus* according to the method discussed in Sect. 2.4. The percent growth inhibition (% GI) of all the dyes was determined and illustrated in Fig. 13. Dye SN5 was found potent against both bacterial strains showing 90 and 95% growth inhibition against *Staphylococcus aureus* and *Escherichia coli* respectively while both SN1 and SN4 dyes showed 90% growth inhibition against *Staphylococcus aureus* only. All the dyes were found inactive against *Aspergillus fumigatus*. Amphotericin B and ofloxacin were used as positive controls for this experiment. These well-known antimicrobial substances were picked because of their proven effectiveness against a variety of pathogens. Ofloxacin, a fluoroquinolone antibiotic, is efficient against a variety of bacteria, whereas amphotericin B, a polyene antifungal medication, is frequently used to treat significant fungal infections. It has been established that a compound's lipophilicity and polarizability, which alternately depend

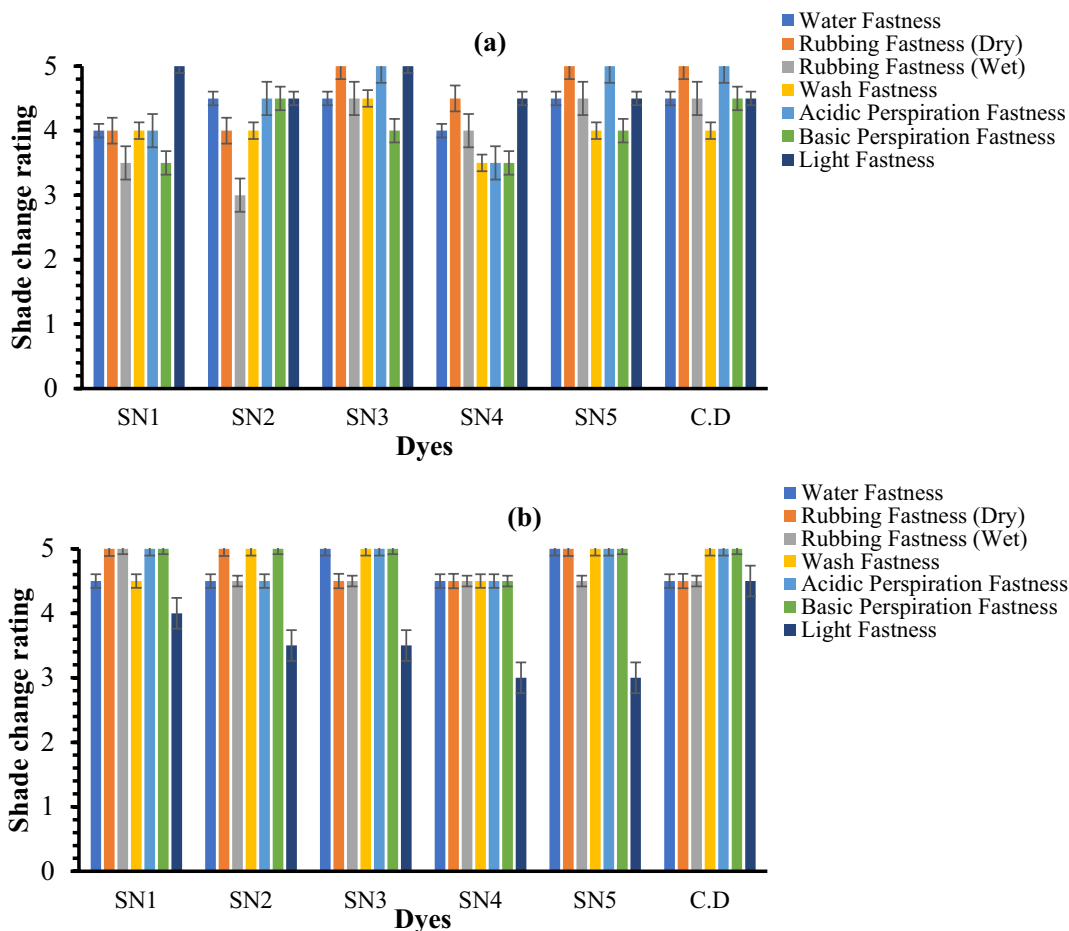


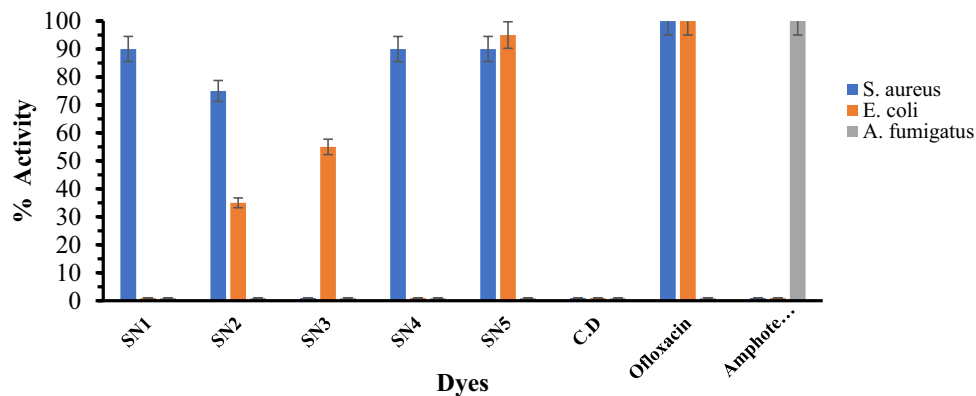
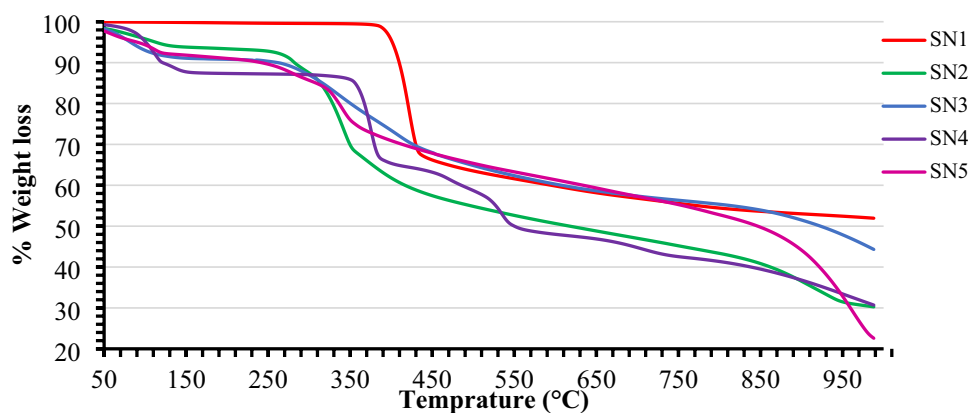
**Fig. 12** Shade change ratings of the dyes (SN1–SN5) on wool (a) and nylon-6 (b) fabrics

**Table 6** Results of cytotoxicity of the synthesized dyes

Dye	Conc. ( $\mu\text{g/ml}$ )	% I/S	IC <sub>50</sub> $\pm$ SD
SN1	30	1.5	Inactive
SN2	30	8.8	Inactive
SN3	30	5.4	Inactive
SN4	30	12.4	Inactive
SN5	30	-0.6	Inactive

Value less than 50% are non-cytotoxic

on the presence of certain functional groups, govern its antimicrobial behavior [44]. Dye **SN5** which showed activity against both the test strains of bacteria has  $\text{NH}_2$  group para to the azo group while it has a hydroxyl and a sulfonic group as well. Dye **SN2**, which showed 75% activity against *Staphylococcus aureus* and 35% against *Escherichia coli*, has similar substituents, but it has the  $\text{NH}_2$  group ortho to the azo group. As it has been already discussed that dye **SN2** predominantly exists in its hydrazo (azonium) tautomeric form while the dye **SN5** mostly exists in its molecular form in a neutral medium. This structural difference could be the possible reason behind their different antimicrobial property. Dye **SN3** has a phenyl ring attached to the nitrogen of the amino group which increases the overall molecular size of the dye. This large molecular size could be the potential cause for its low antimicrobial activity, which may hinder

**Fig. 13** Graphical representation of antimicrobial activity of the dyes (SN1–SN5)**Fig. 14** TGA curve of the acid dyes (SN1–SN5)

the molecule's ability to effectively penetrate the bacterial cell [45, 46]. The commercial dye, which was used to compare the color fastness results of the synthesized dyes, was also tested for antimicrobial activity and found inactive.

### 3.5 Thermal Stability of the Dyes

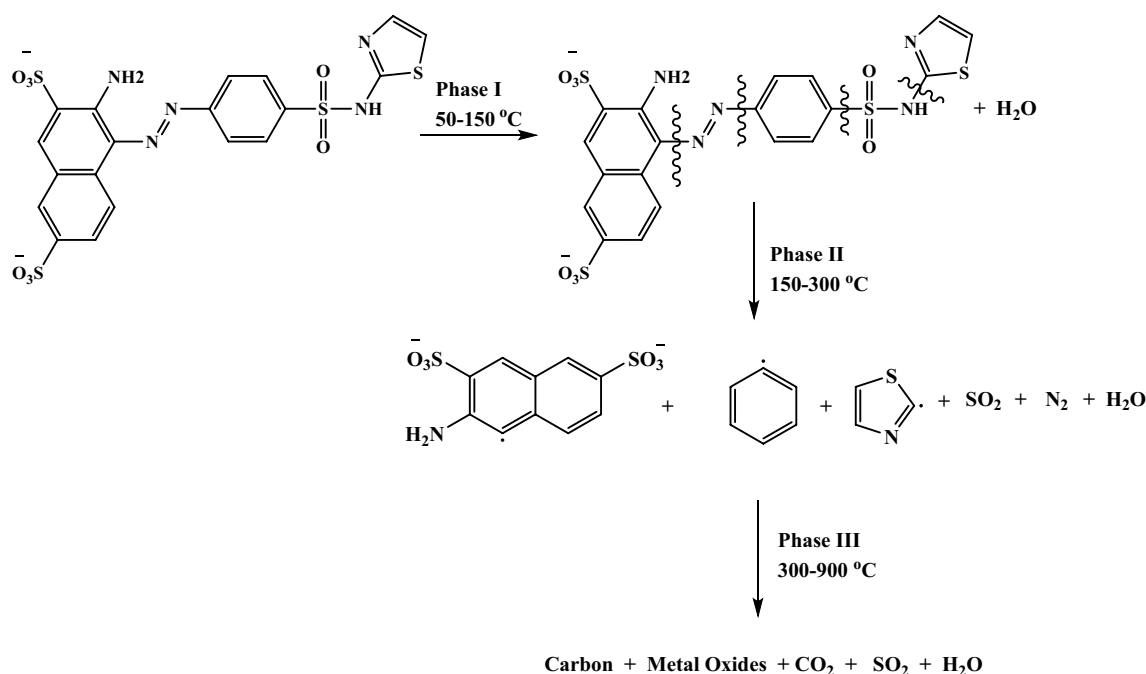
Under controlled conditions, when a sample is subjected to heat, and its weight loss is monitored over time. This process yields valuable data on chemical and physical events, including the release of volatile compounds, thermal breakdown, and phase transitions. The thermal analysis experiment was conducted on the synthesized dyes, the temperature range depicted in Fig. 14, spanning from 50 to 950 °C, was categorized into three distinct phases. In the initial phase of the analysis (phase 1), occurring between 50 and 150 °C, the evaporation of water content occurs. All the dyes exhibited a weight loss of approximately 1–10% during phase 2, which occurs within the temperature range of 150–300 °C. The reduction in weight can be attributed to the degradation of the dye molecules, and chemical rearrangements. Phase 3 encompasses the temperature range of 300–950 °C and is characterized by the decomposition of the dye molecules. Dye **SN1** displayed notably enhanced thermal stability, a characteristic attributed to its greater polar nature. On the other hand, dye **SN5** demonstrated the lowest thermal stability. The presence of two sulfonate groups in dye **SN1** contributed to the formation of

**Table 7** % Reduction in weight of each dye with the temperature rise

Dye	Phase 1 (50–150 °C)	Phase 2 (150–300 °C)	Phase 3 (300–950 °C)	%Residue
SN1	< 1%	< 1%	48%	52%
SN2	6%	6%	58%	30%
SN3	9%	4%	43%	44%
SN4	10%	3%	56%	31%
SN5	7%	7%	63%	23%

stronger intermolecular forces, thereby granting it high thermal stability [47]. The extent of weight loss experienced by each dye as the temperature was elevated within each phase, along with the remaining residue after the analysis is listed in Table 7. The TGA thermal curve depicted in Fig. 14 shows a gradual descent from left to right.

Concerning the fragments observed in the thermogravimetric analysis (TGA) study, an illustrative example of the common fragments of the dye **SN1** during each phase is presented in Scheme 2. Upon subjecting the dye to TGA up to 900 °C, the residual substance appeared as a black powder, indicating extensive decomposition of the dyes at elevated temperatures. This observation is ascribed to the profound thermal degradation experienced by organic compounds under such conditions. The residue predominantly comprises inorganic compounds, such as metal oxides, carbon, or ash, which aligns with the typical behavior of organic compounds when exposed to such high thermal energies [48].

**Scheme 2** An illustrative example of the common fragments of the dye **SN1** during each phase

## 4 Conclusion

A series of sulfathiazole-based mono-azo acid dyes (**SN1–SN5**) were synthesized in good yield. The selection of sulfathiazole was decided after careful examination of its intrinsic antibacterial efficacy. The structures of the resulting dyes were identified using various analytical techniques, and their thermal stability was assessed. Additionally, the influence of pH on the absorption maxima was investigated. These synthetic colorants were then applied on polyamide fabrics (wool and nylon-6) at a 4% *owf* (On Weight of Fabric) shade, and their respective fastness properties were assessed. The findings indicated that these dyes exhibited a favorable level of color fastness on both types of fabrics. The antimicrobial activity of these chromophores was assessed against *Aspergillus fumigatus*, *Escherichia coli*, and *Staphylococcus aureus*. The dye **SN5** demonstrated the highest efficacy against both bacterial strains, while dyes **SN1** and **SN4** showed effectiveness specifically against *Staphylococcus aureus*. A comparison was carried out to assess the fastness and antimicrobial characteristics of the synthesized dyes in relation to a commercially available dye. The results suggest that these dyes could serve as valuable options for coloring a variety of textile products, particularly those utilized in medical and veterinary applications. These dyes were found non-cytotoxic after evaluation on BJ *Human Fibroblast Cells*, which indicates their potential use for the

coloration of non-textile materials, such as cosmetics, food, drugs, and leather.

**Supplementary Information** The online version contains supplementary material available at <https://doi.org/10.1007/s12221-024-00610-8>.

**Acknowledgements** We would like to pay our special regards to Lucky Textile Mills Ltd. (Karachi, Pakistan) for light fastness testing.

**Author contributions** Muhammad Sohail Khan Rafiq: Conceptualization, Methodology, Validation, Investigation, Formal analysis, Software, Visualization, writing – original draft, writing – editing. Abdul Jabbar: Conceptualization, Resources, Supervision, Validation, Writing – review and editing. Saira Faisal: Supervision, Validation, Writing – review and editing. Muhammad Salman: Formal analysis, Software.

**Funding** This research did not receive any specific grant from funding agencies in the public, commercial, or not-for-profit sectors.

**Data availability** Not applicable.

## Declarations

**Conflict of interest** The authors declare that they have no known competing financial interests or personal relationships that could have appeared to influence the work reported in this paper.

**Consent for publication** Not applicable.

## References

1. Y. Zhi-Gang, Z. Chun-Xia, Z. De-Feng, H.S. Freeman, C. Pei-Tong, H. Jie, *Dyes Pigm.Pigm.* **81**(2), 137 (2009). <https://doi.org/10.1016/j.dyepig.2008.09.021>
2. D.P. Chattopadhyay, *Handbook of Textile and Industrial Dyeing*, in *Principles, Processes and Types of Dyes*. ed. by M. Clark (Woodhead Publishing, Sawston, 2011)
3. D.P. Chattopadhyay, *Handbook of Textile and Industrial Dyeing*, in *Principles, Processes and Types of Dyes*. ed. by M. Clark (Woodhead Publishing, Sawston, 2011), pp.515–561
4. V. Moody, H.L. Needles, *Tufted Carpet: Textile Fibers Dyes Finishes and Processes* (William Andrew, Amsterdam, 2005)
5. F.A. Mohamed, T.M. Tawfik, H.M. Ibrahim, *Egypt. J. Chem.* **66**(13), 993 (2023)
6. J. Wu, Q. Li, W. Li, Y. Li, G. Wang, A. Li, H. Li, *J. Cleaner Prod.* **251**, 119694 (2020). <https://doi.org/10.1016/j.jclepro.2019.119694>
7. D.M. Lewis, *Dyestuff fibre Int* **29**, 23 (1999)
8. S. Benkhaya, S. M'rabet, A. El Harfi, *Inorg. Chem. Commun.. Chem. Commun.* **115**, 107891 (2020). <https://doi.org/10.1016/j.inoche.2020.107891>
9. H.B. Slama, A. Chenari Bouket, Z. Pourhassan, F.N. Alenezi, A. Silini, H. Cherif-Silini, T. Oszako, L. Luptakova, P. Golińska, L. Belbahri, *Appl. Sci.* **11**(14), 6255 (2021)
10. F.A. Mohamed, M.S. Bashandy, H. Abd El-Wahab, M.B. Sheier, M.M. El Molla, A.H. Bedair, *Int. J. Adv. Res.. J. Adv. Res.* **2**(7), 248 (2014)
11. M.A. Weaver, L. Shuttleworth, *Dyes Pigm.Pigm.* **3**(2), 81 (1982). [https://doi.org/10.1016/0143-7208\(82\)80016-8](https://doi.org/10.1016/0143-7208(82)80016-8)
12. B. Ravi, J. Keshavayya, V. Kumar, S. Kandgal, *J. Mol. Struct. Struct.* **1204**, 127493 (2020). <https://doi.org/10.1016/j.molstruc.2019.127493>
13. O. Nagaraja, Y.D. Bodke, I. Pushpavathi, S.R. Kumar, *Heliyon* **6**(6), 04245 (2020). <https://doi.org/10.1016/j.heliyon.2020.e04245>
14. B. Manjunatha, Y.D. Bodke, O. Nagaraja, G. Nagaraju, M. Sridhar, *J. Mol. Struct.Struct.* **1246**, 131170 (2021). <https://doi.org/10.1016/j.molstruc.2021.131170>
15. Y. Mi, J. Zhang, X. Han, W. Tan, Q. Miao, J. Cui, Q. Li, Z. Guo, *Int. J. Biol. Macromol.Macromol.* **181**, 572 (2021). <https://doi.org/10.1016/j.ijbiomac.2021.03.109>
16. K. Singh, R. Pal, S.A. Khan, B. Kumar, M.J. Akhtar, *J. Mol. Struct.Struct.* **1237**, 130369 (2021). <https://doi.org/10.1016/j.molstruc.2021.130369>
17. M. Rauf, S. Hisaindee, *J. Mol. Struct.Struct.* **1042**, 45 (2013). <https://doi.org/10.1016/j.molstruc.2013.03.050>
18. H.E. Gaffer, M.E. Mohamed, M.K. Zahran, *Life Sci. J.* **11**(11), 138 (2014)
19. S. Sagheer, A. Jabbar, M.K. Pervez, K. Rani, S. Riaz, *J. Mol. Struct.Struct.* **1250**, 131837 (2022). <https://doi.org/10.1016/j.molstruc.2021.131837>
20. A. Jabbar, S. Riaz, F.A. Navaid, M. Choudhary, *J. Mol. Struct. Struct.* **1195**, 161 (2019). <https://doi.org/10.1016/j.molstruc.2019.05.019>
21. S. Riaz, F.A. Navaid, M.I. Choudhary, A. Jabbar, *J. Mol. Liq.* **287**, 110917 (2019). <https://doi.org/10.1016/j.molliq.2019.110917>
22. S. Riaz, A. Jabbar, S. Khaskheli, S. Sagheer, M.I. Choudhary, *J. Mol. Struct.Struct.* **1272**, 134219 (2023). <https://doi.org/10.1016/j.molstruc.2022.134219>
23. K.A. Amin, H.A. Hameid II., A. Abd Elsttar, *Food Chem. Toxicol. Toxicol.* **48**(10), 2994 (2010). <https://doi.org/10.1016/j.fct.2010.07.039>
24. A. Oving, *J. Biophys. Rev.* **13**(2), 259 (2021). <https://doi.org/10.1007/s12551-021-00795-9>
25. A. Tačić, V. Nikolić, L. Nikolić, I. Savić, *Adv. Technol.* **6**(1), 58 (2017). <https://doi.org/10.5937/savteh1701058T>
26. D.R. Patel, K.C. Patel, *Dyes Pigm.Pigm.* **90**(1), 1 (2011). <https://doi.org/10.1016/j.dyepig.2010.10.013>
27. L. Tolosa, M.T. Donato, M.J. Gómez-Lechón, *Volume 1250: Protocols in In Vitro Hepatocyte Research* (Springer, Berlin, 2015)
28. M. Mannerström, T. Toimela, J.R. Sarkanen, T. Heinonen, *Basic Clin. Pharmacol. Toxicol.Clin. Pharmacol. Toxicol.* **121**, 109 (2017). <https://doi.org/10.1111/bcpt.12790>
29. P. Price, T.J. McMillan, *Cancer Res.* **50**(5), 1392 (1990)
30. N. Sultanova, T. Makhmoor, Z. Abilov, Z. Parween, V. Omurkamzinova, M.I. Choudhary, *J. Ethnopharmacol.Ethnopharmacol.* **78**, 201 (2001). [https://doi.org/10.1016/S0378-8741\(01\)00354-3](https://doi.org/10.1016/S0378-8741(01)00354-3)
31. R. Naz, A. Bano, *Asian Pac. J. Trop. Biomed.* **2**(12), 944 (2012). [https://doi.org/10.1016/S2221-1691\(13\)60004-0](https://doi.org/10.1016/S2221-1691(13)60004-0)
32. Z. Mohammadkhodaei, J. Mokhtari, M. Nouri, *Color. Technol.* **126**(2), 81 (2010). <https://doi.org/10.1111/j.1478-4408.2010.00230.x>
33. H.F. Huang, W. Ma, B.T. Tang, S.F. Zhang, *Chin. Chem. Lett.* **21**(4), 417 (2010). <https://doi.org/10.1016/j.ccllet.2009.11.010>
34. H. Günther, N.M.R. Spectroscopy, *Basic Principles* (Concepts and Applications in Chemistry, John Wiley and Sons, London, 2013)
35. T. Sutradhar, A. Misra, *J. Phys. Chem. A* **122**(16), 4111 (2018). <https://doi.org/10.1021/acs.jpca.8b00261>
36. L. Antonov, S. Stoyanov, *Dyes Pigm.Pigm.* **28**(1), 31 (1995). [https://doi.org/10.1016/0143-7208\(94\)00076-E](https://doi.org/10.1016/0143-7208(94)00076-E)
37. C.E. de Melo, M. Dominguez, M.C. Rezende, V.G. Machado, *Dyes Pigm.Pigm.* **184**, 108757 (2021). <https://doi.org/10.1016/j.dyepig.2020.108757>



38. M. Yazdanbakhsh, M. Gahi, A. Mohammadi, *J. Mol. Liq.* **144**(3), 145 (2009). <https://doi.org/10.1016/j.molliq.2008.10.013>
39. A. Mohammadi, M.R. Yazdanbakhsh, L. Farahnak, *Spectrochim Acta, Part A.* **89**, 238 (2012). <https://doi.org/10.1016/j.saa.2011.12.062>
40. T. Stoyanova, S. Stoyanov, L. Antonov, V. Petrova, *Dyes Pigm. Pigm.* **31**(1), 1 (1996). [https://doi.org/10.1016/0143-7208\(95\)00095-X](https://doi.org/10.1016/0143-7208(95)00095-X)
41. D.R. Matazo, R.A. Ando, A.C. Borin, P.S. Santos, *J. Phys. Chem. A* **112**(19), 4437 (2008). <https://doi.org/10.1021/jp800217c>
42. D. Debnath, S. Roy, B.-H. Li, C.-H. Lin, T.K. Misra, *Spectrochim Acta. Part A.* **140**, 185 (2015). <https://doi.org/10.1016/j.saa.2014.12.027>
43. F. Walker, *The Chemistry and Application of Dyes* (Springer, Boston, 1990)
44. Z. Akhtar, S.I. Ali, N. Abbas, M. Ali, M.Y. Khan, S.A. Hasan, S. Ahmed, S. Manzoor, Z. Lutfi, *J. Chem. Soc. Pak.* **42**(5), 783 (2020). <https://doi.org/10.52568/000688>
45. M. Zaidan, A. Noor Rain, A. Badrul, A. Adlin, A. Norazah, I. Zakiah, *Trop. Biomed. Biomed.* **22**(2), 165 (2005)
46. N. Özbek, H. Katurcioğlu, N. Karacan, T. Baykal, *Bioorg. Med. Chem. Med. Chem.* **15**(15), 5105 (2007). <https://doi.org/10.1016/j.bmc.2007.05.037>
47. H.L. Nguyen, T. Bechtold, *J. Cleaner Prod.* **315**, 128195 (2021). <https://doi.org/10.1016/j.jclepro.2021.128195>
48. M. Kazem-Rostami, *J. Therm. Anal. Calorim. Calorim.* **140**, 613 (2020). <https://doi.org/10.1007/s10973-019-08884-4>

Springer Nature or its licensor (e.g. a society or other partner) holds exclusive rights to this article under a publishing agreement with the author(s) or other rightsholder(s); author self-archiving of the accepted manuscript version of this article is solely governed by the terms of such publishing agreement and applicable law.